Revealing the Behavior of Photons in a Birefringent Interferometer

Zhi-Yuan Zhou,[1,2,3,*,†] Shi-Kai Liu,[1,2,*] Shi-Long Liu,[1,2] Yin-Hai Li,[1,2,3] Yan Li,[1,2] Chen Yang,[1,2] Zhao-Huai Xu,[1,2] Guang-Can Guo,[1,2] and Bao-Sen Shi[1,2,3,‡]

[1]*CAS Key Laboratory of Quantum Information, USTC, Hefei, Anhui 230026, China*

[2]*Synergetic Innovation Center of Quantum Information and Quantum Physics, University of Science and Technology of China, Hefei, Anhui 230026, China*

[3]*Wang Da-Heng Collaborative Innovation Center for Science of Quantum Manipulation and Control, Heilongjiang Province and Harbin University of Science and Technology, Harbin 150080, China*

(Received 1 January 2018; published 26 June 2018)

The interferometer is one of the most important devices for revealing the nature of light and for precision optical metrology. Although many experiments were performed for probing photon behavior in various configurations, a complete study of photon behavior in a birefringent interferometer has not been performed, to our knowledge. By using an environmental turbulence immune Mach-Zehnder interferometer, we observe tunable photonic beatings by rotating a birefringent crystal versus the temperature of the crystal for both the single photon and two photons. Furthermore, the two-photon interference fringes beat 2 times faster than the single-photon interference fringes. This beating effect is used to determine the thermal dispersion coefficients of the two principal refractive axes with a single measurement: the two-photon interference shows superresolution and high sensitivity. Obvious differences between two-photon and single-photon interference are also revealed in unbalanced situations. In addition, the influence of the photon bandwidth on the beating behaviors that come from polarization-dependent decoherence is also investigated. Our findings will be important for better understanding the behavior of two-photon interference in a birefringent interferometer and for precision optical metrology with quantum enhancement.

DOI: 10.1103/PhysRevLett.120.263601

Since Young's pioneering work on double-slit interference in 1807 [1,2], the optical interferometer has been a basic tool of modern science and technology used to study the fundamental nature of light, and it has had broad applications in all scientific fields. For example, the interferometer has been used to study the wave-particle duality of photons [3–5] and the nonclassical effects of quantum sources [6–8]. The fundamental understanding of photon interference has been debated since Dirac [9]. In Dirac's view, a photon can interfere only with itself. Such a viewpoint encounters some problems when one explains two-photon interference generated from a type-I or a type-II spontaneous parametric down-conversion process [10,11]. Later, physicists updated Dirac's viewpoint, as a pair of photons interferes only with the pair itself [11,12]. Once we know how a photon behaves in a certain interference process, we can better apply this behavior for high-precision metrology based on photon interference. Measurements of most physical quantities, including position, displacement, distance, angle, optical dispersion, and optical path length, often depend on decoding parameters from specific interference fringes or patterns [13–18]. How to obtain stable interference fringes and obtain more parameters in a single interference fringe is the long pursued aim in interference based precision optical metrology. For instance, in gravitational-wave detectors like LIGO [19], which must be placed in a high-cost vacuum to achieve high stability. Also, in a recent work, Smith and Shih reported on turbulence-free double-slit experiments based on two-photon interference [12].

In this Letter, an intrinsic stable interferometer is used which is based on a modified Sagnac interferometer. Since light beams in the two arms of the interferometer are slightly tilted and in counterpropagation configurations, both light beams have nearly the same sensitivity to environmental turbulence such as temperature fluctuation and vibrations. Therefore, the phase changes of the two arms are canceled and the relative phase between the two arms can hold for hours. By inserting birefringent crystals in this intrinsic stable interferometer, the behavior of photon interference is studied and revealed for the first time. A complete quantum description of a birefringent Mach-Zehnder interferometer (MZI) is performed in this Letter, which is rather different from previous studies [20]. Some interesting results are revealed behind the general theory. A quantum beating versus crystal temperature for both single-photon and two-photon interference is observed. In addition, the beating intensity can be tuned by rotating the crystal, and the two-photon interference fringes beat 2 times faster than the single-photon interference fringes. This beating effect is used to determine the thermal dispersion coefficients of the two principal refractive axes with a single measurement.

Moreover, the two-photon input case shows superresolution and higher sensitivity; we also find that the beating behavior is strongly dependent on the bandwidth of the input photons, which comes from polarization decoherence of the photon propagation in the birefringent crystal; this behavior of photon interference has not been observed before.

The general theoretical models will be given first. A simplified diagram is shown in Fig. 1, in which two birefringent potassium titanyl phosphate (KTP) crystals have been inserted into a modified MZI. One of these crystals, designated KTP2, is used to compensate for the optical path length differences in the interferometer. The other KTP crystal (KTP1) is mounted on a rotation stage to rotate its position with respect to the horizontal polarization direction. The photon operators at the output ports (P4, P5) are connected to those at the input ports (P0, P1) through the transformations provided by the beam splitters and the birefringent crystals. By assuming that the photon's coherence length is much greater than both the imbalance of the interferometer and the optical path length difference between the optical axes of the birefringent crystal, the photon operators ($\hat{A}_4$, $\hat{A}_5$) at ports P4 and P5 can be expressed in terms of the operators ($\hat{A}_0$, $\hat{A}_1$) at ports P0 and P1 using the following expression [21] (for details, see the Supplemental Material [22]):

$$\hat{A}_4 = \frac{1}{\sqrt{2}}(\hat{A}_2' + i\hat{A}_3') = F_1(\hat{A}_0, \hat{A}_1)\vec{e}_H + G_1(\hat{A}_0, \hat{A}_1)\vec{e}_V,$$
$$\hat{A}_5 = \frac{1}{\sqrt{2}}(i\hat{A}_2' + \hat{A}_3') = F_2(\hat{A}_0, \hat{A}_1)\vec{e}_H + G_2(\hat{A}_0, \hat{A}_1)\vec{e}_V, \tag{1}$$

where $\hat{F}_1$, $\hat{G}_1$, $\hat{F}_2$, $\hat{G}_2$ are expressed as follows:

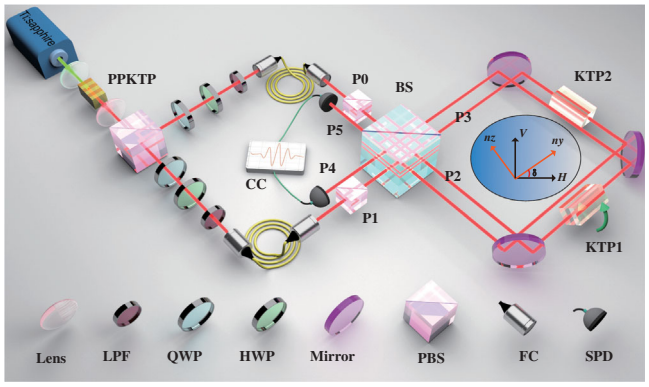

FIG. 1. Experimental setup for photon pair generation and photon interference. PPKTP, periodically poled potassium titanyl phosphate crystal; PBS, polarizing beam splitter; SMF, single-mode fibers; FC, fiber collimators; QWP, quarter-wave plates; HWP, half-wave plates; LPF, long pass filters; SPD, single-photon detectors.

$$\hat{F}_1 = -\frac{1}{2}(T-\alpha)\hat{A}_0 + \frac{i}{2}(T+\alpha)\hat{A}_1, \qquad \hat{G}_1 = \frac{\beta}{2}(\hat{A}_0 + i\hat{A}_1),$$
$$\hat{F}_2 = \frac{i}{2}(T+\alpha)\hat{A}_0 + \frac{1}{2}(T-\alpha)\hat{A}_1, \qquad \hat{G}_2 = \frac{i\beta}{2}(\hat{A}_0 + i\hat{A}_1), \tag{2}$$

where $|\alpha|^2 + |\beta|^2 = 1$, $\alpha = \cos^2\delta e^{i\Delta\varphi_y} + \sin^2\delta e^{i\Delta\varphi_z}$, $\beta = \cos\delta\sin\delta(e^{i\Delta\varphi_y} - e^{i\Delta\varphi_z})$, and δ is the rotation angle of KTP1; $\vec{e}_H$ and $\vec{e}_V$ represent the unit vectors in the two orthogonal polarization directions; and $\Delta\varphi_i = 2\pi n_i(\lambda, T)L/\lambda (i = y, z)$ represents the optical phase changes along the y and z axes of the birefringent crystal, where L is the crystal length, λ is the wavelength of the photon, and T is the crystal temperature.

For the single-photon input case, the single-photon count rates R_4, R_5 at ports 4 and 5 can be calculated to be

$$R_4 = \frac{1}{2}[1 + \cos^2\delta\cos(\Delta\varphi_y - \Delta\varphi_c) + \sin^2\delta\cos(\Delta\varphi_z - \Delta\varphi_c)], \tag{3}$$

$$R_5 = \frac{1}{2}[1 - \cos^2\delta\cos(\Delta\varphi_y - \Delta\varphi_c) - \sin^2\delta\cos(\Delta\varphi_z - \Delta\varphi_c)]. \tag{4}$$

For the two-photon input case, the corresponding count rate $R_{4,5}$ between ports 4 and 5 can be calculated as follows:

$$R_{4,5} = \frac{1}{4}\Big\{1 + \cos^4\delta\cos(2\Delta\varphi_y - 2\Delta\varphi_c) + \sin^4\delta\Big[\cos(2\Delta\varphi_z - 2\Delta\varphi_c) + \frac{1}{2}\cos(\Delta\varphi_y + \Delta\varphi_z - 2\Delta\varphi_c)\Big]\Big\}. \tag{5}$$

Equations (3), (4), and (5) are the main results for input of the narrow-band photon pair. The results for input of a broadband photon pair will be discussed in the following text and in the Supplemental Material [22].

We now experimentally demonstrate the predictions that were described in the theoretical models above. The experimental setup is shown in Fig. 1. The photon pair is generated using a type-II periodically poled KTP crystal (PPKTP), which has a length of 2 cm. The crystal has a poling period of 46.2 μm, and the degenerate phase matching temperature for the 775 nm pump beam is 30.030($\pm$0.002) °C. The orthogonally polarized photons in a pair are separated by the polarizing beam splitter (PBS), and the photons are then coupled into single-mode fibers (SMFs). The pump beam is removed using long pass filters (LPFs) before the photons are coupled into the SMFs. The polarizations of the photons in the SMFs are controlled using two pairs of half-wave plates (HWPs) and

quarter-wave plates (QWPs). The photons that are released from the two SMFs are first polarization purified using two PBSs and are then injected into a self-stable MZI, which contains two KTP crystals; one KTP crystal is used for the measurements, while the other compensates for the optical path length differences between the two arms of the MZI. The self-stable MZI is based on a tilted Sagnac loop, where the clockwise and counterclockwise beams have a traverse distance of 10 mm. The two KTP crystals have dimensions of $5 \times 5 \times 8$ mm, and both end faces are antireflection coated for 1550 nm. Both crystals are x cut such that the beams propagate along the x axes of the crystal. KTP1 is used for the measurements, while KTP2 is used for compensation, and the temperature of KTP2 is kept at a constant $22.300(\pm 0.002)$ °C. The temperature of KTP1 can be tuned from $17.810(\pm 0.002)$ °C to $45.670(\pm 0.002)$ °C. The temperatures of the two crystals are controlled using two homemade temperature controllers with a temperature stability of ± 0.002 °C. The delay between the two-photon pairs is controlled using a one-dimensional translation stage. The output photons at ports 4 and 5 are connected to two free-running InGaAs single-photon detectors (SPDs; ID220, 20% quantum efficiency, 5 μs dead time). The output signals from the two SPDs are sent to a coincidence measurement device (TimeHarp 260, 0.4 ns coincidence window).

We first characterize the photonic beating effects for the heralded single-photon and two-photon maximally path-entangled number states ($N00N$ states). The bandwidth of the photon is 1.3 nm without spectral filtering. The Hong-Ou-Mandel (HOM) interference fringes for the photons without filtering and with a 0.5 nm filter are shown in Fig. 2, and we see that nearly perfect HOM interference characteristics are observed in both cases, with visibilities of $97.42 \pm 0.16\%$ and $98.71 \pm 0.29\%$, respectively. For HOM measurements, paths P2 and P3 are directly coupled to two SMFs for detection, and the delays between the photons are tuned by a one-dimensional stage mounted on the signal arm. The HOM dip shapes are determined by the spectrum of the photon pair [10,23]: for the unfiltered case, the spectrum of the photon should be a sinc^2 function [see Eq. (s11) of the Supplemental Material [22]], while for the filtered case, the two-photon spectrum is a Gaussian function. In the unfiltered case, the pump power is 8.4 mW, the single count rates are approximately 62 and 77 kHz for the signal and idler photons, respectively, and the dark count rate is approximately 3 kHz. For the filtered case, the pump power is approximately 16 mW, and the single count rates for the signal and idler photons are 90 and 56 kHz, respectively. For detailed characteristics of the photon sources, please refer to Refs. [24,25].

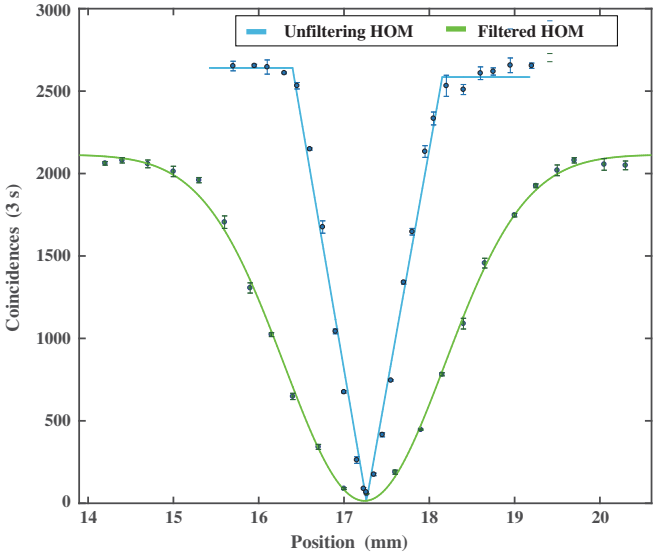

FIG. 2. HOM interference fringes for the unfiltered and filtered cases. In the unfiltered case, the theoretical curve used to fit the data is a triangle function; in the filtered case, the theoretical curve used to fit the data is Gaussian.

When the photons in each pair reach the BS simultaneously, a two-photon $N00N$ state is generated after the two output ports of the BS because of bunching effects in HOM interference. The single-photon and two-photon beating curves versus temperature for the different rotation angles of the KTP1 crystal are shown in Fig. 3. The panels on the left (from bottom to top) show the beating curves of the two-photon input for rotation angles of $\delta = 0, \pi/6, \pi/4, \pi/3, \pi/2$. The panels on the right show the corresponding beating curves for the heralded single photon. The rotation angles of $\delta = 0, \pi/2$ represent cases in which the input photon polarization coincides with the y and z optical axes

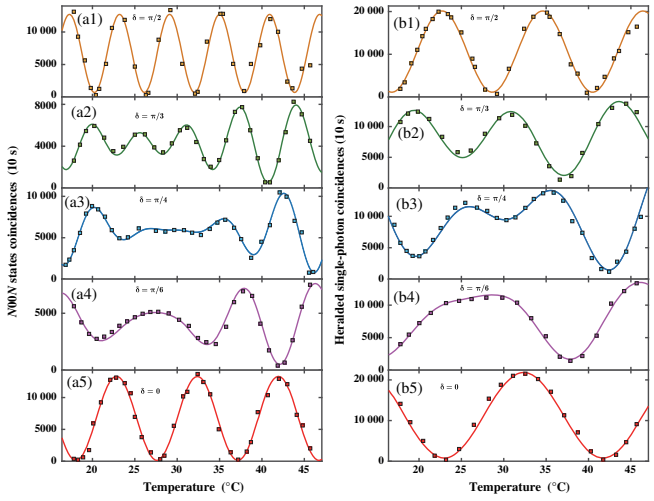

FIG. 3. Photonic beating versus temperature for the two-photon input case and the heralded single-photon input case. The panels on the left (from bottom to top) represent the two-photon cases at rotation angles of $\delta = 0, \pi/6, \pi/4, \pi/3, \pi/2$. The panels on the right represent the corresponding heralded single-photon input case. The measurement time is 10 s. Different offsets in each of the interference fringes come from the different initial phases between the two arms of the interferometer.

of the birefringent crystal. The two-photon and single-photon visibilities for the two cases are $(98.01 \pm 0.18)\%$ and $(94.75 \pm 0.27)\%$, and $(93.09 \pm 0.23)\%$ and $(90.87 \pm 0.34)\%$, respectively. In these two cases, the two- (single-) photon case yields thermal dispersions $(dn_y/dT, dn_z/dT)$ of $(1.027 \pm 0.019) \times 10^{-5}/\mathrm{K}$ $[(1.041 \pm 0.044) \times 10^{-5}/\mathrm{K}]$ and $(1.680 \pm 0.019) \times 10^{-5}/\mathrm{K}$ $[(1.651 \pm 0.035) \times 10^{-5}/\mathrm{K}]$ for the y (z) axis. The other curves show the beating behavior of the optical properties along the two axes, and we can determine the optical properties along both axes from any single measurement of this type of beating curve. For example, when $\delta = \pi/3$, the thermal dispersions that were obtained for two (single) photons for axes y and z were $(0.980 \pm 0.067) \times 10^{-5}/\mathrm{K}$ $[(0.928 \pm 0.104) \times 10^{-5}/\mathrm{K}]$ and $(1.592 \pm 0.013) \times 10^{-5}/\mathrm{K}$ $[(1.594 \pm 0.037) \times 10^{-5}/\mathrm{K}]$, respectively.

Another important feature of the beating curve is that the temperature oscillation period of the beating curve for the two-photon case is 2 times faster than that of the heralded single-photon cases, which indicates higher measurement resolution when a high-photon-number entanglement state is used in measurements. We should point out that the environment temperature fluctuation is higher than $\pm 0.002\,^{\circ}\mathrm{C}$ (usually $\pm 0.5\,^{\circ}\mathrm{C}$), but the relative phase of the interferometer remains unchanged during the measurement time durations, which indicates that the self-stable MZI is immune to environmental turbulence.

Next, we discuss the effects of the imbalance of the MZI on the interference fringes for both the two-photon input and the heralded single-photon input when the rotation angle of KTP1 is $\delta = 0$. Three cases are studied: (I) when the optical lengths are equal, the crystal KTP2 is also aligned along the y axes, and the optical path difference between the two interfering arms is 0 mm; (II) when the imbalance of the MZI is within the single-photon coherence length, which is realized by rotating KTP2 by 90°, and the optical path difference is 0.66 mm; (III) when the imbalance of the MZI is greater than the coherence length of the single photon, which is realized by removing the crystal KTP2, and the optical path length difference is 5.87 mm. In these three cases, the two-photon interference fringes for both the two-photon and single-photon cases are shown in Fig. 4. The visibilities for these three cases for the two-photon and single-photon inputs are $97.98 \pm 0.19\%$ and $94.26 \pm 0.46\%$, $98.18 \pm 0.14\%$ and $93.09 \pm 0.23\%$, and $54.20 \pm 0.97\%$ and 0, respectively. Obvious differences between the two-photon interference fringes and the single-photon interference fringes are reveals. The single-photon interference visibility decreases with an increase of optical path difference in the MZI, while the two-photon interference visibility is immune to small optical path differences. As mentioned in the introduction, the single-photon case involves interference with itself [9], and two-photon interference is the interference of the photon pair itself [11,12]. The two-photon coherence length is the same as the

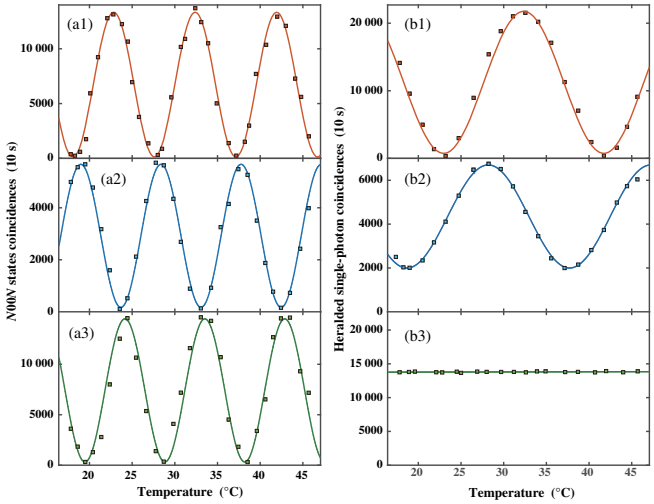

FIG. 4. Interference fringes of the two-photon (left panel) and single-photon (right panel) cases for $\delta = 0$ with increasing optical path length difference. The optical path length differences in order from top to bottom are 0, 0.66, and 5. 87 mm.

coherence length of the pump laser beam, which is at the ~kilometer level. Therefore, small optical path differences in the MZI have no effect on the two-photon interference fringes. By contrast, since the single-photon coherence length is at the 2 mm level, the interference fringes are very sensitive to optical path length differences in the MZI.

Finally, we study the effects of the photon bandwidth on the interference fringes; the polarization decoherence of the photon is dependent on the photon bandwidth. For photons with an angular spectral bandwidth of $\Delta\omega = 2\sqrt{\ln 2}\sigma$ and a spectral distribution of $f^2(\omega_i) = (1/\sqrt{\pi}\sigma)\exp[-(\omega_i - \omega_{i0})^2/\sigma^2]$, the single count at port 4 and the coincidence count between ports 4 and 5 are given as follows:

$$R_4 = \frac{1}{2}\left[1 + \cos^2\delta\cos\left(\frac{dk_y}{dT}L\Delta T\right) + \sin^2\delta\exp\left(-\frac{D^2L^2\sigma^2}{4}\right)\cos\left(\Delta\varphi + \frac{dk_z}{dT}L\Delta T\right)\right], \tag{6}$$

$$R_{45} = \frac{1}{2}\left\{1 + \cos^4\delta\cos\left(2\frac{dk_y}{dT}L\Delta T\right) + \sin^4\delta\cos\left(2\frac{dk_z}{dT}L\Delta T + 2\Delta\varphi\right) + \frac{1}{2}\sin^4\delta\cos\left[\left(\frac{dk_z}{dT} + \frac{dk_y}{dT}\right)L\Delta T + \Delta\varphi\right] \times \exp\left(-\frac{D^2L^2\sigma^2}{4}\right)\right\}, \tag{7}$$

where $\Delta\varphi = [k_z(\omega_0, T_0) - k_y(\omega_0, T_0)]L$, $D = \partial k_z/\partial\omega - \partial k_y/\partial\omega = 1/v_{gz} - 1/v_{gy}$, and $\Delta T = T - T_0$. These parameters can be obtained from the Sellmeier equations for the y and z axes [26,27]. Detailed derivations of Eqs. (6) and (7) can be found in the Supplemental Material [22] and in Ref. [28]. For a photon spectrum with the form of a sinc^2 function, analytical expressions are given by Eqs. (s29)–(s34) in the Supplemental Material [22]. The experimental results for the unfiltered case for both the two-photon and single-photon input cases when $\delta = \pi/4$ are shown in Fig. 5. The interference visibility decreases as the bandwidth increases. When photon bandwidth is increasing, the time overlapping of photon projected in the two optical axes is decreasing. For photons with large bandwidths, the last terms in Eqs. (6) and (7) can be ignored.

A full theoretical and experimental description of photon interference in a birefringent interferometer is presented in this Letter. With careful design of a self-stable MZI, how a photon behaves in the MZI is revealed in detail. Photonic beating behavior versus crystal temperature is observed for both the single photon and two photons. This beating behavior is used to determine the optical properties along both crystal axes with a single measurement. The two-photon interference fringes oscillate twice as fast as those of a single photon, which indicates superresolution measurement capabilities in the multiphoton entangled state. The differences in single- and two-photon interference behavior in an unbalanced MZI verify the viewpoint that the single photon involves interference with itself, and two-photon interference is the interference of the photon pair itself. We should point out that the single-photon input case is not limited to a single photon: the same would be true for lasers, which would simplify the setups in practical applications. The present system is not limited to determination of the thermal dispersion of a birefringent crystal and can also be used to determine the wavelength dispersion [29] and electro-optical coefficient of the birefringent crystal. This work will thus be of great importance for understanding the nature of photon and for precision optical metrology.

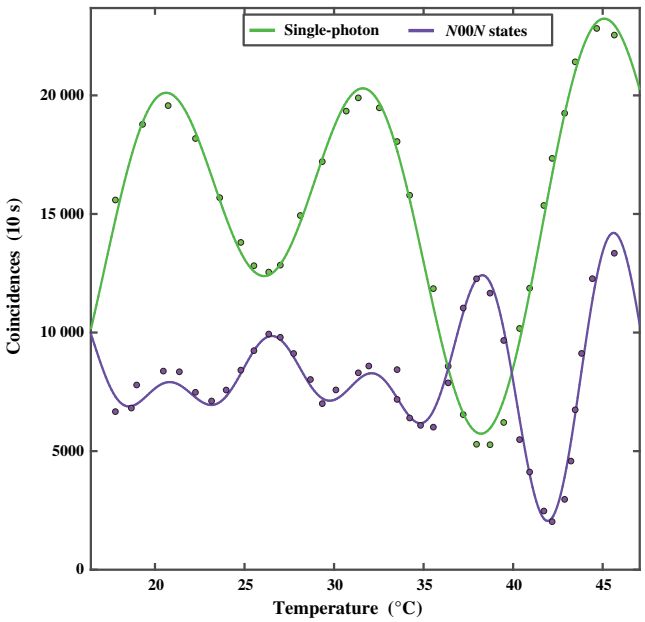

FIG. 5. Two-photon and single-photon interferences without filtering when $\delta = \pi/4$. The coincidence time is 10 s. The parameters used for the fitting $L = 8$ mm, dn_y/dT, dn_z/dT are $1.03 \times 10^{-5}/\mathrm{K}$ and $1.620 \times 10^{-5}/\mathrm{K}$, respectively; $\sigma = \pi/\sqrt{\ln 2} \times 50\,\mathrm{GHz}$; $D = 0.947$ ps/mm.

This work is supported by the National Natural Science Foundation of China (NSFC) (Grants No. 61435011, No. 61525504, and No. 61605194); the National Key Research and Development Program of China (Grant No. 2016YFA0302600); the Anhui Initiative In Quantum Information Technologies (Grant No. AHY020200); the China Postdoctoral Science Foundation (Grant No. 2016M590570); and the Fundamental Research Funds for the Central Universities.

*These authors contributed equally to this work.
†Corresponding author.
zyzhouphy@ustc.edu.cn
‡Corresponding author.
drshi@ustc.edu.cn

[1] T. Young, *A Course of Lectures on Natural Philosophy and the Mechanical Arts* (J. Johnson, London, 1807).
[2] E. Hecht, *Optics* (Addison-Wesley, Reading, MA, 2002).
[3] V. Jacques, E. Wu, F. Grosshans, F. Treussart, P. Grangier, A. Aspect, and J. Roch, Experimental realization of Wheeler's delayed-choice Gedanken experiment, Science **315**, 966 (2007).
[4] R. Ionicioiu and D. R. Terno, Proposal for a Quantum Delayed-Choice Experiment, Phys. Rev. Lett. **107**, 230406 (2011).
[5] Z.-Y. Zhou, Z.-H. Zhu, S.-L. Liu, Y.-H. Li, S. Shi, D.-S. Ding, L.-X. Chen, W. Gao, G.-C. Guo, and B.-S. Shi, Quantum twisted double-slits experiments: confirming wavefunctions' physical reality, Science bulletin **62**, 1185 (2017).
[6] X. Ma, J. Kofler, and A. Zeilinger, Delayed-choice Gedanken experiments and their realizations, Rev. Mod. Phys. **88**, 015005 (2016).
[7] C. K. Hong, Z. Y. Ou, and L. Mandel, Measurement of Subpicosecond Time Intervals between Two Photons by Interference, Phys. Rev. Lett. **59**, 2044 (1987).
[8] A. Danan, D. Farfurnik, S. Bar-Ad, and L. Vaidman, Asking Photons Where They Have Been, Phys. Rev. Lett. **111**, 240402 (2013).
[9] P. Dirac, *The Principle of Quantum Mechanics* (Oxford University Press, New York, 1930).
[10] Morton H. Rubin, D. N. Klyshko, Y. H. Shih, and A. V. Sergienko, Theory of two-photon entanglement in type-II optical parametric down-conversion, Phys. Rev. A **50**, 5122 (1994).

[11] T. B. Pittman, D. V. Strekalov, A. Migdall, M. H. Rubin, A. V. Sergienko, and Y. H. Shih, Can Two-Photon Interference Be Considered the Interference of Two Photons?, Phys. Rev. Lett. **77**, 1917 (1996).
[12] T. A. Smith and Y. Shih, Turbulence-Free Double-Slit Interferometer, Phys. Rev. Lett. **120**, 063606 (2018).
[13] V. Giovannetti, S. Lloyd, and L. Maccone, Quantum-enhanced measurements: Beating the standard quantum limit, Science **306**, 1330 (2004).
[14] A. R. Thompson, J. M. Moran, and G. W. Swenson, Jr., *Interferometry and Synthesis in Radio Astronomy* (John Wiley & Sons, New York, 2001).
[15] P. R. Saulson, *Fundamentals of Interferometric Gravitational Wave Detectors* (World Scientific, Singapore, 1994).
[16] D. C. Williams, *Optical Methods in Engineering Metrology* (Chapman and Hall, London, 1993).
[17] D. D. Nolte, *Optical Interferometry for Biology and Medicine* (Springer, New York, 2011).
[18] M. E. Brezinski, *Optical Coherence Tomography: Principles and Applications* (Academic Press, New York, 2006).
[19] B. P. Abbott *et al.* (LIGO Scientific and Virgo Collaborations), Observation of Gravitational Waves from a Binary Black Hole Merger, Phys. Rev. Lett. **116**, 061102 (2016).
[20] J. G. Rarity, P. R. Tapster, E. Jakeman, T. Larchuk, R. A. Campos, M. C. Teich, and B. E. A. Salch, Two-Photon Interference in a Mach-Zehnder Interferometer, Phys. Rev. Lett. **65**, 1348 (1990).
[21] K. Edamatsu, R. Shimizu, and T. Itoh, Measurement of the Photonic de Broglie Wavelength of Entangled Photon Pairs Generated by Spontaneous Parametric Down-Conversion, Phys. Rev. Lett. **89**, 213601 (2002).
[22] See Supplemental Material at http://link.aps.org/supplemental/10.1103/PhysRevLett.120.263601 for details of the theoretical derivations.
[23] A. M. Branczyk, Hong-Ou-Mandel interference, arXiv:1711.00080.
[24] Y. Li, Z.-Y. Zhou, D.-S. Ding, and B.-S. Shi, CW-pumped telecom band polarization entangled photon pair generation in a Sagnac interferometer, Opt. Express **23**, 28792 (2015).
[25] Z.-Y. Zhou, S.-L. Liu, S.-K. Liu, Y.-H. Li, D.-S. Ding, G.-C. Guo, and B.-S. Shi, Superresolving Phase Measurement with Short-Wavelength $N00N$ States by Quantum Frequency Up-Conversion. Phys. Rev. Applied **7**, 064025 (2017).
[26] F. Kong and F. N. C. Wong, Extended phase matching of second-harmonic generation in periodically poled $KTiOPO_4$ with zero group-velocity mismatch, Appl. Phys. Lett. **84**, 1644 (2004).
[27] K. Fradkin, A. Arie, A. Skliar, and G. Rosenman, Tunable midinfrared source by difference frequency generation in bulk periodically poled $KTiOPO_4$ Appl. Phys. Lett. **74**, 914 (1999).
[28] Z.-Y. Zhou, D.-S. Ding, B.-S. Shi, X.-B. Zou, and G.-C. Guo, Characterizing dispersion and absorption parameters of metamaterial using entangled photons, Phys. Rev. A **85**, 023841 (2012).
[29] F. Kaiser, P. Vergyris, D. Aktas, C. Babin, L. Labonté, and S. Tanzilli, Quantum enhancement of accuracy and precision in optical interferometry, arXiv:1701.01621.